Hindawi
Advances in Polymer Technology
Volume 2019, Article ID 8625325, 10 pages
https://doi.org/10.1155/2019/8625325

WILEY | Hindawi

Research Article

Crystallinity and Reinforcement in Poly-L-Lactic Acid Scaffold Induced by Carbon Nanotubes

Guoyong Wang,[1] Fangwei Qi,[1] Wenjing Yang,[1] Youwen Yang,[1] Chongxian He,[1] Shuping Peng ,[2,3] and Cijun Shuai [1,4]

[1]*Jiangxi University of Science and Technology, Ganzhou 341000, China*
[2]*NHC Key Laboratory of Carcinogenesis and The Key Laboratory of Carcinogenesis and Cancer Invasion of the Chinese Ministry of Education, Xiangya Hospital, Central South University, Changsha, Hunan, China*
[3]*Cancer Research Institute, School of Basic Medical Sciences, Central South University, Changsha, Hunan, China*
[4]*State Key Laboratory of High Performance Complex Manufacturing, Central South University, Changsha 410083, China*

Correspondence should be addressed to Shuping Peng; shuping@csu.edu.cn and Cijun Shuai; shuai@csu.edu.cn

Received 24 August 2019; Accepted 24 October 2019; Published 12 December 2019

Guest Editor: Yu Tao

Poly-L-Lactic Acid (PLLA) is a bioabsorbable implant material due to its favorable biocompatibility and inherent degradability, while the insufficient mechanical strength hinders its further bone repair application. In present work, carbon nanotubes (CNTs) were introduced into PLLA scaffolds fabricated via selective laser sintering. It was found that the crystallinity of PLLA increased considerably since CNTs could promote the orderly stacking of its molecular chains, thereby improving the mechanical strength of PLLA scaffold. Furthermore, the fracture surface analysis revealed that CNTs acted as a bridge across the cracks and hindered their further expansion. Moreover, CNTs pulled out from the matrix to consume a large amount of fracture energy, which enhanced the resistance to external forces. As a consequence, the compressive strength, Vickers hardness and tensile strength of the scaffold were enhanced by 22.7%, 58.8% and 17.6%, respectively. Besides, the cells exhibited good attachment, spreading and proliferation on the scaffold. This study demonstrated that PLLA/CNTs scaffold was a promising candidate as bone implant.

1. Introduction

Poly-L-Lactic Acid (PLLA) has been recognized as a promising bone repair material due to its good biocompatibility and desirable biodegradability [1–3]. It is able to degrade into lactic acid by hydrolysis, and then metabolize to water and carbon dioxide, which can be removed from the body via normal metabolic pathways [4, 5]. Given the attractive characteristic of PLLA, it has received the approval from the Food and Drug Administration for implant application [6]. Recently, numerous investigations have attempted to utilize PLLA as temporary bone implant [7, 8]. Nevertheless, these studies indicated that PLLA exhibited poor mechanical properties, especially for load bearing, which significantly hinder its further bone repair application [9].

Incorporation of reinforcement, such as nanoparticles [10, 11], nanowires [12], graphene nanoplatelets [13] and carbon nanotubes (CNTs) [14], is a workable approach to enhance the mechanical performance of polymer matrix. Among them, CNTs exhibited superior mechanical performance, including high strength, modules and hardness [15]. Meanwhile, CNTs have been proved to be of favorable biocompatibility and osteoprotective property [16]. Li et al. introduced CNTs into polycarbonate microfibrils, and enhanced the tensile strength and elastic modulus by 20%, 40%, respectively [17]. Wang et al. proved that CNTs as a nanofiller for PLLA could overcome the brittleness, with the elongation at break and the impact strength improved 205% and 30%, respectively [18]. Mesgar et al. used CNTs to reinforce the chitosan scaffolds, which enhanced the modulus to 11 times [19]. Luo et al. fabricated multi-walled carbon nanotubes polycaprolactone composite scaffolds using the solution evaporation technique [20]. *In vivo* results showed that the composite scaffolds had good bone bioactivity.

In present study, CNTs were incorporated into PLLA to enhance the mechanical properties. The PLLA/CNTs composite scaffold was prepared by selective laser sintering (SLS) process. Previous researchers have fabricated PLLA/CNTS scaffold via phase separation method [21], electrospinning technique [22], freeze-drying method [23], etc. Comparing

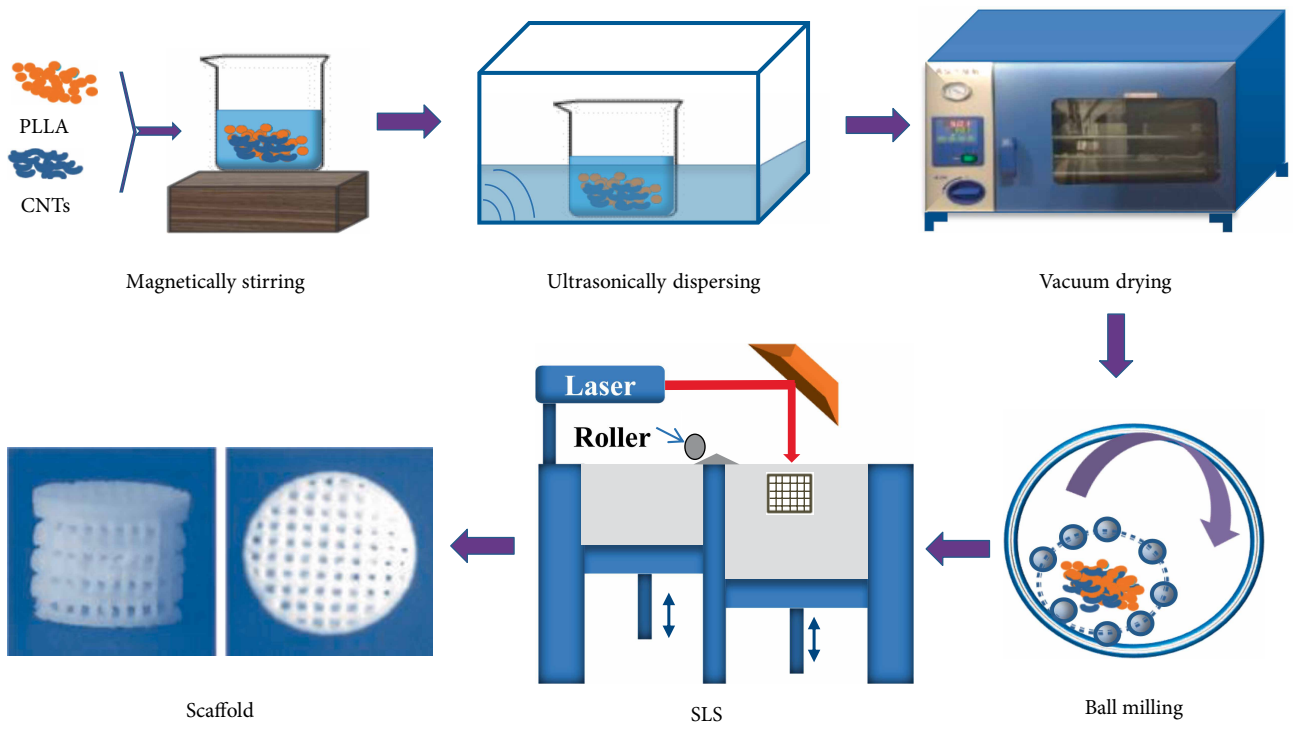

Figure 1: Schematic of the scaffold preparation process.

with previous methods, selective laser sintering exhibits great advantages including accurate control of the pore structure and strong ability to customize for specific defect sites [24–27]. The microstructure evolution and mechanical behavior of the composite scaffold were investigated. The effect of CNTs on the mechanical behavior was clarified in detail. In addition, the biocompatibility of the PLLA/CNTs scaffold was studied via *in vitro* cell experiments.

2. Materials and Methods

2.1. Materials. CNTs with the outside diameter ranging from 4 to 6 nm and the length ranging from 10 to 20 μm was provided from Chengdu Organic Chemicals Co. Ltd. The PLLA powder was purchased from Shenzhen Polymtek Biomaterial Co. Ltd. (Shenzhen, China) with average molecular weights 150 mol/g, purity more than 99%, and density 1.25 g/cm^3.

2.2. Preparation of PLLA/CNTs Composite Scaffold. The detailed fabrication process of PLLA/CNTs scaffold was depicted in Figure 1. Specifically, a certain quantity of CNTs was first added into anhydrous ethanol solution. The suspension was then magnetically stirred and ultrasonically dispersed for 6 h. Subsequently, the PLLA powder was added into the above CNTs suspension. Afterwards, the PLLA/CNTs suspension was magnetically stirred and ultrasonically dispersed for 12 h. The suspension was then dried in a vacuum oven at 45°C until the powder weight maintained stable. Finally, the PLLA/CNTs mixed powder was obtained after ball milling for 1 h.

The PLLA/CNTs composite scaffold was prepared using a self-developed SLS system. The detailed preparation process was described as follows: Firstly, the 3D model matching the bone scaffold was designed. The model was imported into the SLS system to create the slice file; secondly, the composite powder was spread on the workbench; thirdly, the composite powder was selectively sintered layer-by-layer according to the above slice file. The optimal process parameters of SLS process were determined by pilot experiments (laser power 2.5 W, scanning speed 120 mm/s, scanning distance 0.1 mm and layer thickness 0.1 mm). The obtained scaffolds with nominal CNTs of 0, 0.25, 0.5, and 1.0 wt.% were named as PLLA, PLLA/0.25CNTs, PLLA/0.5CNTs, and PLLA/1.0CNTs, respectively. The pore size and strut size of the sintered scaffolds were about 650 μm and 450 μm, respectively, as shown in Figure 1. In general, porous bone scaffolds was able to provide a favorable microenvironment for cell into-growth [28, 29].

2.3. Microstructural Characterization. The chemical characteristic of the samples was qualitatively evaluated by Fourier transform infrared spectroscopy (FTIR, Bruker Tensor 27). The samples and dried potassium bromide powder were mixed and grounded into fine powder. Then, they were pressed into discs in a mold. The FTIR spectra were obtained with a resolution of 2 cm^{-1} from 500 to 3000 cm^{-1} at room temperature. Subsequently, the intensity of transmittance and the characteristic peaks was measured. Raman spectroscopy was obtained using a Raman spectrometer (Renshaw, UK) with a laser excitation of 532 nm and scans range between 400 and 2500 cm^{-1}.

Polarized optical microscope (POM, Olympus Co., Japan) was used to investigate the crystalline morphology of PLLA/CNTs composites. The phase structure was investigated using an X-ray diffractometer (XRD, DMAX 2500, Japan Science Co., Japan) equipped with Cu Ka source. The data was recorded ranging from 10° to 50°.

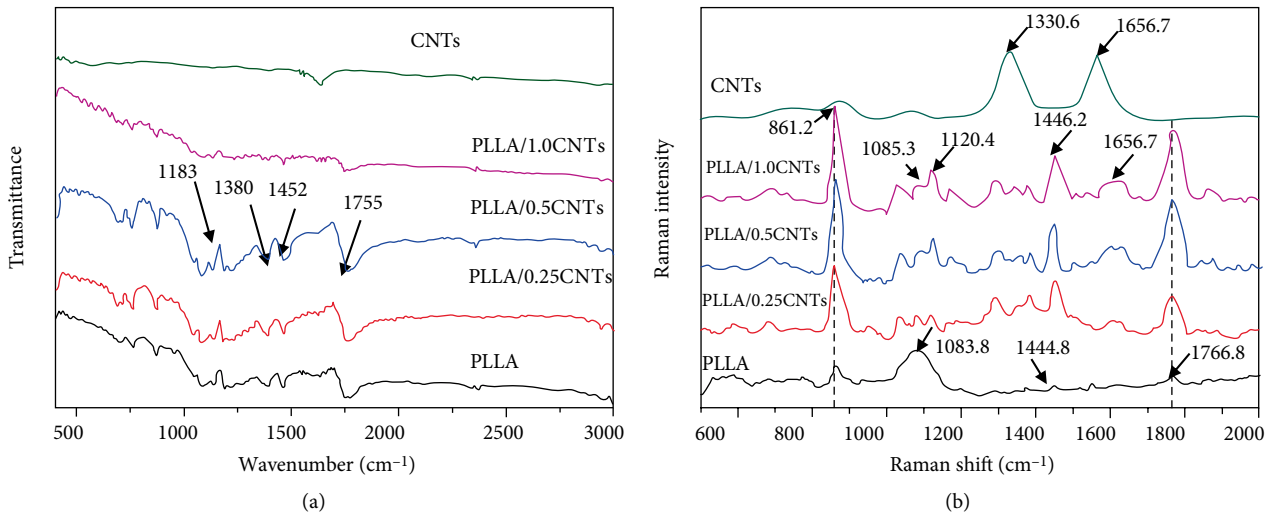

Figure 2: (a) FTIR and (b) Raman spectra of CNTs, neat PLLA, and PLLA/CNTs scaffolds.

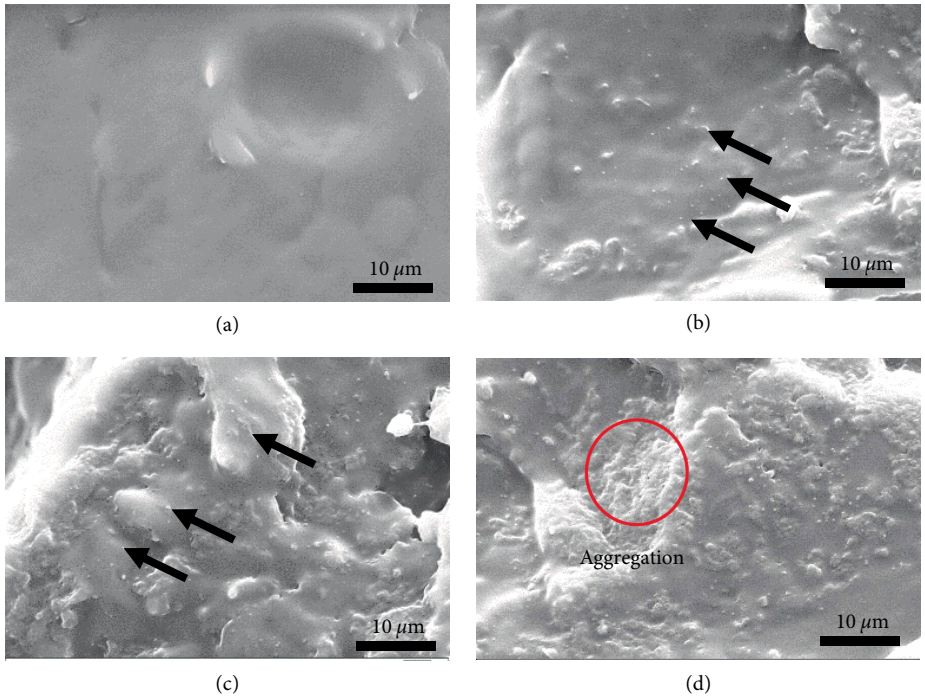

Figure 3: SEM showing the fracture surface of (a) PLLA, (b) PLLA/0.25CNTs, (c) PLLA/0.5CNTs, and (d) PLLA/1.0CNTs scaffolds.

2.4. Mechanical Tests. The Vickers hardness tester (TMVS-1, Beijing TIME High Technology Co. Ltd) was applied to measure the hardness. Three different measurements were carried out for each sample. A mechanical testing machine (WD-D1, LTD, China) was applied to perform the tensile and compressive tests. The tensile specimens (width 5 mm, length 20 mm) was subjected to tensile load until they were broken, and the compressive specimens with porous structure ($10 \times 10 \times 5$ mm^3) were subjected to compression load until they were crushed. The fracture surface morphologies of the scaffolds after tensile tests were observed using a scanning electron microscope (Phillips XL30, Eindhoven, Netherlands). Before SEM observation, the surface of samples was coated with gold for 2 min in a sputter coater.

2.5. Cell Experiments. MG63 cells were cultured in Dulbecco's Modified Eagle Medium supplemented with 10% fetal bovine serum and 1% (v/v) streptomycin/penicillin condition at 37°C (5% humid CO_2). The culture medium was changed every 2 days. Prior to cell seeding, the PLLA and PLLA/CNTs scaffold ($10 \times 10 \times 2$ mm^3) were sterilized under UV irradiation for 24 h. The incubate medium was renewed every day. The MG63 cells were seeded on the PLLA and PLLA/CNTs scaffolds with a density of 10^5 cells per well. After 1, 4 and 7 days, the specimens were rinsed three times using phosphate buffer solution (PBS) in order to remove nonadherent cells. The cell morphology on scaffolds with different culture time was observed by SEM.

The cell viability was assessed using live/dead staining after culture for 1, 4, 7 days. In brief, the cells were stained with

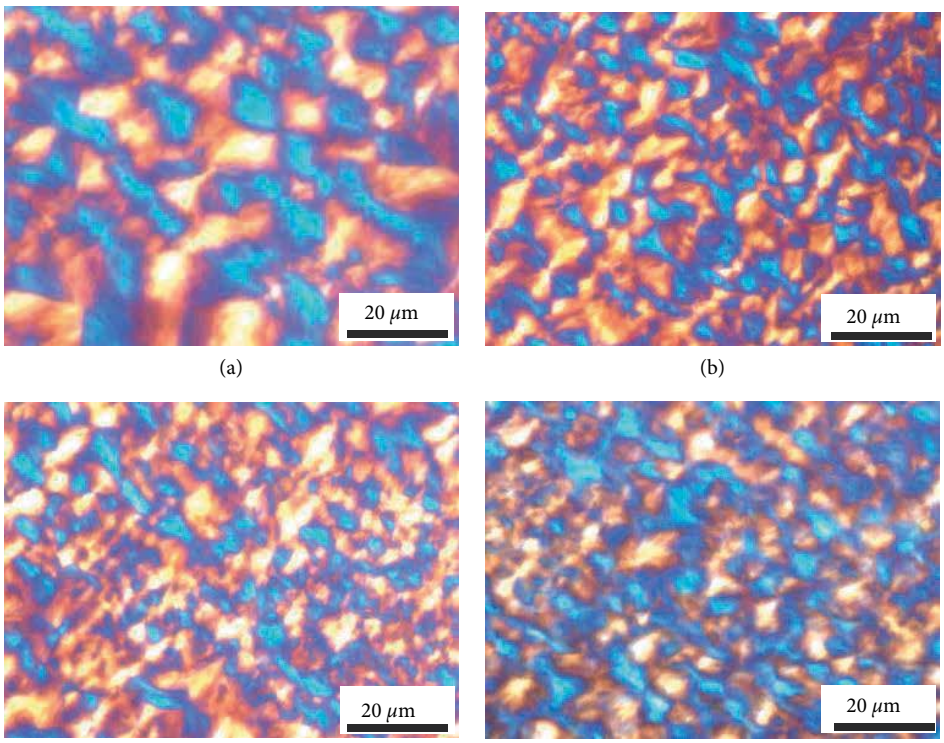

Figure 4: POM of (a) PLLA, (b) PLLA/0.25CNTs, (c) PLLA/0.5CNTs and (d) PLLA/1.0CNTs scaffolds.

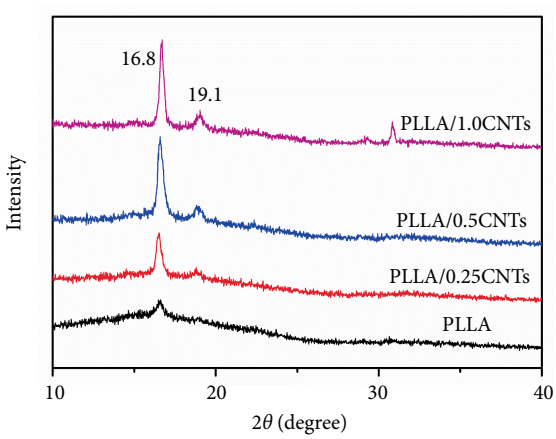

Figure 5: XRD patterns of CNTs, PLLA and PLLA/CNTs composite scaffolds.

2 μg/mL Calcein-AM and Ethidium homodimer-1 reagents for 20 min at 37°C. Then, the stained cells were refreshed with PBS and observed with fluorescence microscope (BX60, Olympus, Japan).

The proliferation of MG63 cells was further evaluated using cells counting kit-8 (CCK-8) assays. Cells were seeded on the scaffolds for 1, 4 and 7 days. Then, 40 μL of CCK-8 solution were added to every well and incubated for 4 h at 37°C. Then the optical density (OD) was measured at 450 nm by a spectrophotometric micro plate reader. Each sample testing was carried out for three times.

2.6. Statistical Analysis. All the experimental data were recorded using at least three separate operations, and expressed as means ± standard deviation. In all statistical analysis, it is considered to be significant with P value less than 0.05.

3. Results and Discussion

3.1. Characterization of the PLLA/CNTS Composite Scaffolds. The FTIR spectra of CNTs, PLLA and PLLA/CNTs scaffolds were displayed in Figure 2(a). As was expected, there was a peak presented at 1635 cm^{-1}, which was assigned to the stretching vibrations of C=C bonds in the CNTs. For PLLA, there were two obvious peaks at 1751 and 1452 cm^{-1}, which was ascribed to the C=O stretching vibrations of its carboxyl groups [30]. The peak located at 1380 cm^{-1} was assigned to the bending vibrations of $-CH_3$ groups [31]. There was a weak broad band appearing at 1183 cm^{-1} which was associated to C–O stretching vibration [32]. Compared with PLLA, there were no new peaks or peak shift in the FTIR spectra of PLLA/CNTs scaffolds.

The Raman measurements were used to further reveal the structural stability of the CNTs during the SLS process. The Raman spectra of CNTs, PLLA and PLLA/CNTs scaffolds were recorded, with results shown in Figure 2(b). It could be found that there were two distinct characteristic peaks observed at 1330.6 and 1656.7 cm^{-1}, which was ascribed to the D- and G-bands of CNTs, respectively. Generally, the D-band was related to the degree of disorder of CNTs, while the G- band was attributed to the in-plane motion of the sp^2 carbon atom

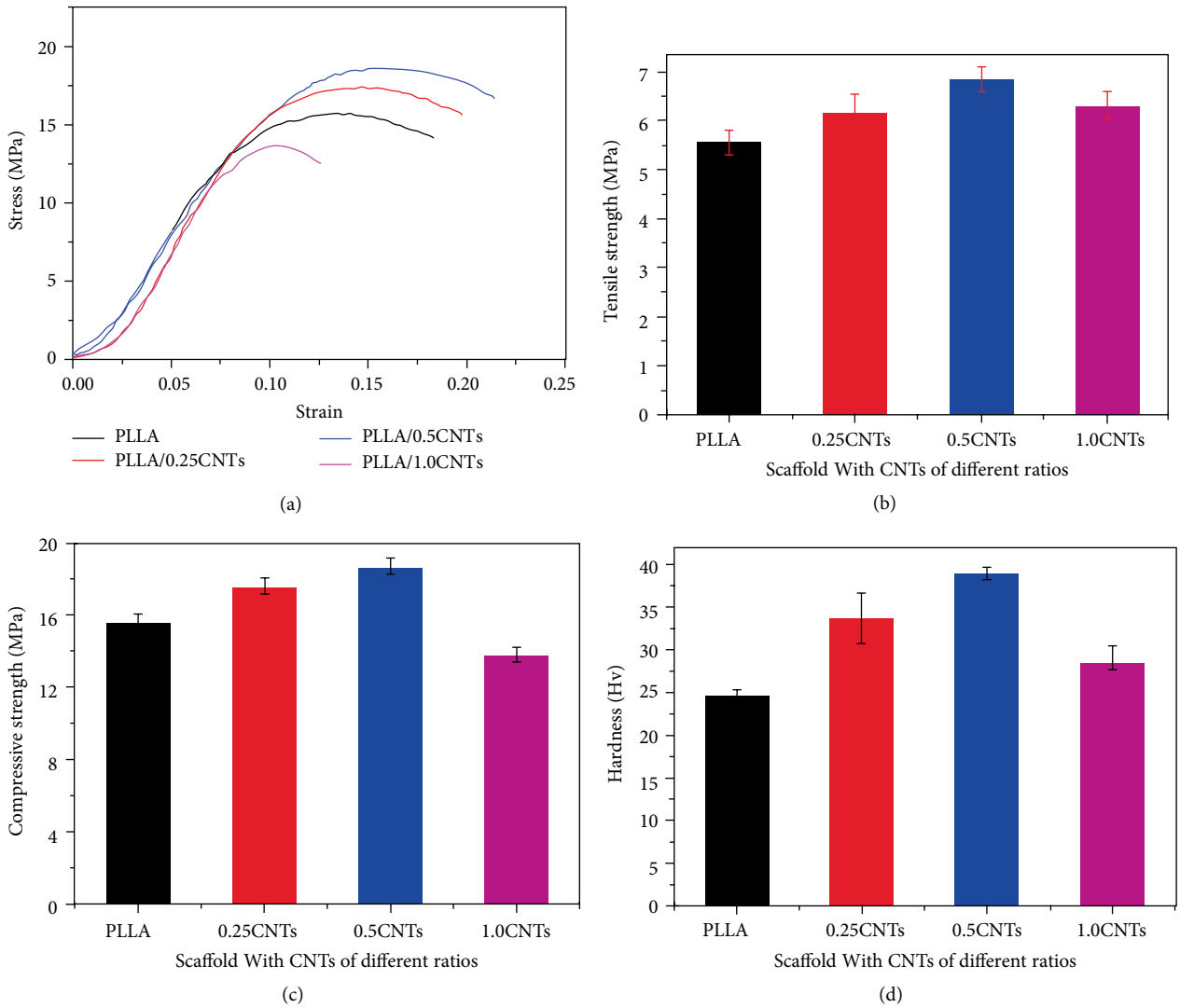

FIGURE 6: Tensile stress-strain curves (a), tensile strength (b), compressive strength (c), and hardness of PLLA and PLLA/CNTs composite scaffolds (d).

[4, 33]. PLLA exhibited three characteristic peaks at 859.6, 1083.8 and 1444.8 cm^{-1}, which were attributed to C–CH_3 stretching, –CH_3 rocking mode and –CH_3 asymmetric bending mode, respectively [34]. For the Raman spectrum of PLLA/CNTs scaffolds, they presented combined characteristic peaks of PLLA and CNTs. The D and G modes of the scaffolds exhibited no noticeable shifts as compared with the spectrum of CNTs. However, the PLLA resonances in the scaffolds included C–CH_3 stretching (861.2 cm^{-1}), –CH_3 rocking mode (1085.3 cm^{-1}), and –CH_3 asymmetric bending mode (1446.2 cm^{-1}) were red-shifted by 1.6, 1.5 and 1.4 cm^{-1}, respectively, as compared with the pure PLLA scaffold [4]. It might be due to the interaction between PLLA and CNTs during SLS.

The brittle fractured surfaces of PLLA/CNTs scaffolds were observed, as shown in Figure 3. PLLA exhibited an obvious brittle fracture with relative flat morphology. As a comparison, there were some micro-fibers on the fractured surface of the PLLA/0.5CNTs scaffold. The CNTs uniformly distributed in the PLLA matrix. The number of micro-fibers increased with the CNTs contents increasing to 0.5 wt.%. However, the agglomeration occurred with CNTs further increasing to 1.0 wt.%.

The crystalline morphology of PLLA/CNTs was investigated using POM, with results displayed in Figure 4. Clearly, PLLA exhibited large spherulites morphology with a typical maltese cross shape. As CNTs gradually increased to 0.5 wt.%, the size of the spherulites decreased considerably, accompanying with the significantly increased density. The results indicated that CNTs acted as heterogeneous nucleating agents and promoted the orderly arrangement, thus accelerating the crystallization of PLLA. Nevertheless, as the CNTs reached 1.0 wt.%, relatively coarsened spherulites were observed in the matrix, indicated the reduced nucleation ability of CNTs for composite matrix. Previous studies revealed that as nanoparticles exceeded a certain content, the ability to promote PLLA nucleation would decrease, which was believed to be related to their agglomeration in PLLA matrix [35].

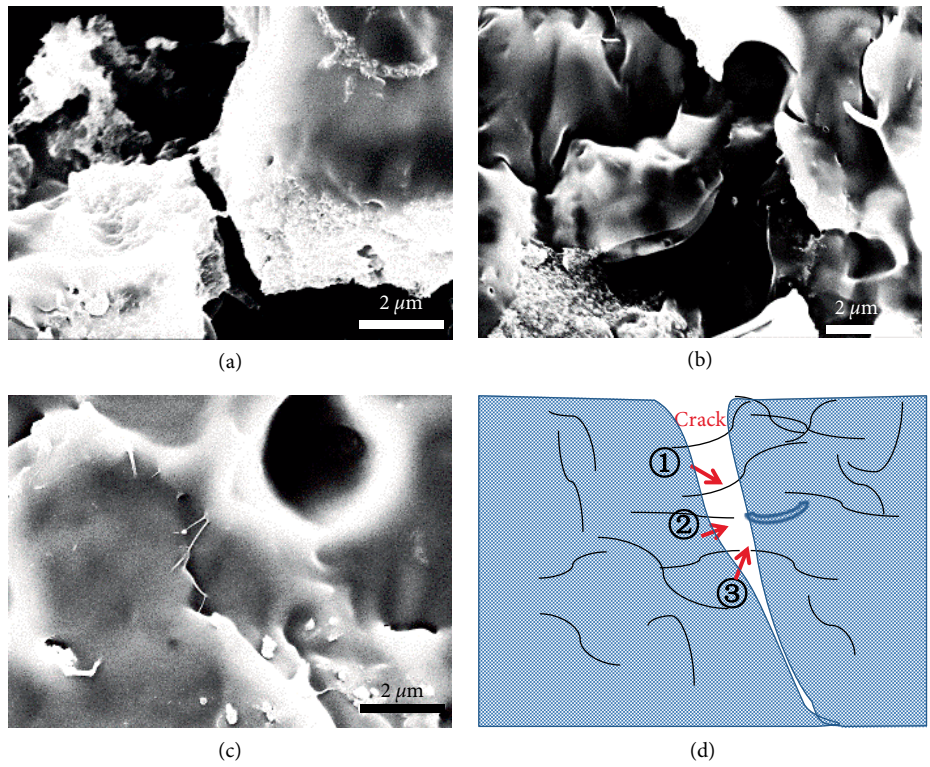

Figure 7: The introduced (a) bridging, (b) pulling out and (c) pinning effect of CNTs in PLLA scaffold. (d) Models of reinforcement mechanisms.

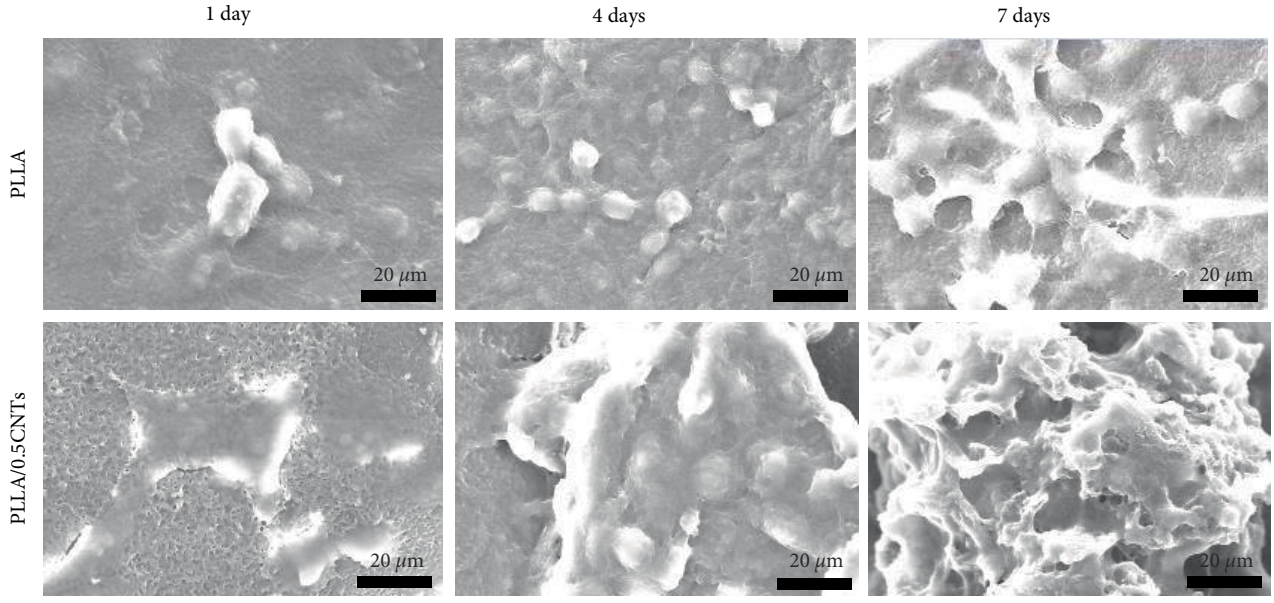

Figure 8: SEM images of the MG63 cells cultured on scaffolds for 1, 4 and 7 days.

The XRD patterns of PLLA and PLLA/CNTs were shown in Figure 5. Obviously, there were two strong diffraction peaks located at $2\theta = 16.8°$ and 19.1° [36], which indicated the occurrence of cold crystallization of PLLA [37]. The XRD patterns of the PLLA/CNTs scaffold still kept the characteristic peaks of PLLA, which indicated that the incorporation of CNTs did not exert a significant influence on the crystalline structure of PLLA. However, the intensity and sharpness of these peaks gradually increased with CNTs increasing, which indicated that the degree of crystallization of polymer composite was enhanced due to the heterogeneous nucleation of CNTs [30].

3.2. Mechanical Properties. Bone scaffolds require appropriate mechanical strength to provide structural support for

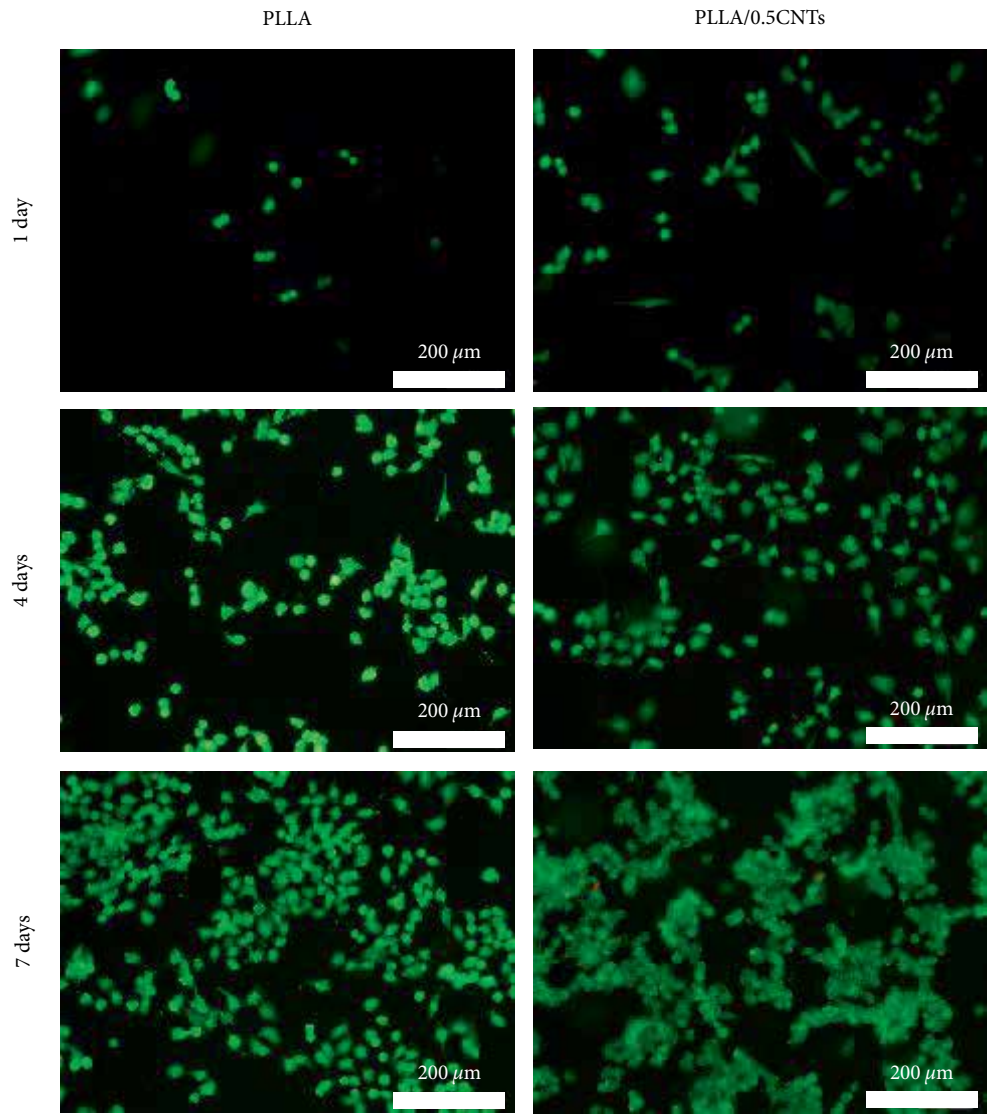

Figure 9: Representative fluorescence images of MG63 cells cultured on scaffolds for 1, 4 and 7 days.

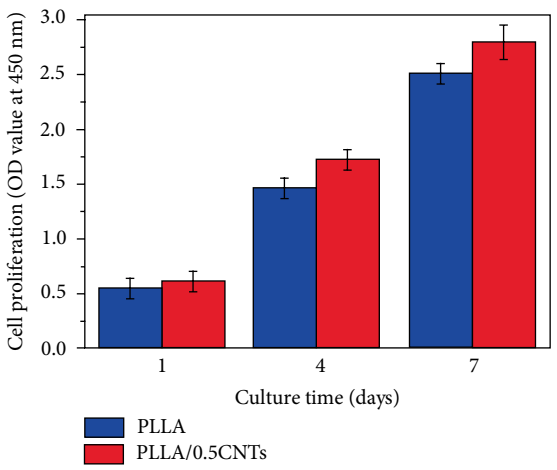

Figure 10: The obtained OD value using CCK-8 assays after 1, 4, 7 days' culture.

the newly formed tissue during bone repair [38, 39]. The mechanical properties of PLLA and PLLA/CNTs scaffolds were evaluated through compressive, hardness and tensile tests, with results shown in Figure 6. The typical compressive stress-strain curves were depicted in Figure 6(a). It could be found that all the samples exhibited the brittle characteristic. As the external force exceeded a certain degree during the compression, the scaffolds were directly fractured without yielding [40]. The compressive strengths derived from their compressive stress-strain curves were shown in Figure 6(b). The compressive strengths of PLLA/CNTs scaffolds increased by 22.7% (from 5.5 MPa to 6.82 MPa) with CNTs increasing to 0.50 wt.%. This could be ascribed to the fact that CNTs could act as a reinforced phase in the PLLA matrix [41]. However, there was a slight decrease in compressive strength with CNTs further increasing to 1.0 wt.%, which might be due to the aggregation of CNTs. It was well established that bone scaffolds should have sufficient mechanical strength to match

the surrounding connective bone. Usually, the compressive strength of the human cancellous bone and cortical bone were in the range of 2–12 MPa and 130–180 MPa, respectively [42]. In this work, the optimal compressive strength of PLLA/CNTs scaffolds was 6.8 MPa, which was in the range of cancellous bone and lower than cortical bone. Therefore, the PLLA/CNTs scaffolds have a potential application in bone repair.

The Vickers hardness and tensile strength of all specimens was shown in Figures 6(c) and 6(d), respectively. Similarly, the Vickers hardness and tensile strength of PLLA/0.5CNTs scaffolds increased to 38.9 Hv and 18.6 MPa, which was increased by 58.8% and 17.6%, respectively. Therefore, the addition of CNTs presented a positive role in enhancing the mechanical properties of PLLA scaffold.

In this work, the CNTs could act as a pinning action to hinder the crack propagation. This was due to the crack in the composite was difficult to deflect during the expansion process and could only continue in the original direction [43]. Thus, the CNTs immediately adjacent to the crack tip did not break, but created a bridging effect between the cracks [44, 45]. The typical crack bridge in the crack surface contact region was shown in Figure 7(a). This bridging effect would offset a part of the tensile stress, thereby hindering the further expansion of the crack. On the other hand, CNTs, as one dimensional material, exhibited significant fiber properties [46]. In this case, the CNTs were pulled out of the matrix during the tensile fracture of the composite scaffolds, thereby consuming a large amount of external energy [47]. As shown in Figure 7(b), some CNTs pulled out from the matrix, whose direction tended to align with the direction of the applied load. Besides, CNTs were embedded into PLLA matrix, which formed the pinning effects. The schematics of pulling out, bridging and crack deflection are shown in Figure 7(d). Furthermore, the increase in the crystallinity of PLLA also had a positive effect on their mechanical properties [48]. However, with the CNTs contents further increasing to 1.0 wt.%, they aggregated in the PLLA matrix, thus failing to enhance the mechanical properties of PLLA/CNTs scaffolds.

3.3. Cytocompatibility. Good biocompatibility was of great significance for the bone implants [49–51]. In present study, the PLLA/0.5CNTs scaffold with optimal mechanical properties was used to further evaluate the cytocompatibility, with the PLLA scaffold as control. The morphologies of cells adhered on scaffolds after cultivating for 1, 4, 7 days were observed by SEM, as shown in Figure 8. After 1 day' culture, cells began to spread on the PLLA/0.5CNTs scaffold with apparent cytoplasmic extensions, indicating a strong adhesion. As culture time increasing to 4, 7 days, the adhered cells on the PLLA/0.5CNTs scaffold increased significantly and overlapped with each other. Additionally, the cells on the PLLA/0.5CNTs scaffold presented much longer filopodia as compared with those on PLLA scaffold. It was indicated that PLLA/0.5CNTs scaffold was more beneficial for cell adhesion.

Stained fluorescent pictures of cells incubated on PLLA/0.5CNTs and PLLA scaffolds for various periods were exhibited in Figure 9. Herein, green represented live cells, whereas red represented dead cells. Clearly, nearly no dead cells were observed for all the samples during cell incubation. In particular, the cells exhibited typical fusiform shape after culture for 1 day, revealing that the cells growth normally on the scaffold. After further incubation for 4, 7 days, cells have expanded into filopodia, and formed numerous extracellular matrix. At the same time, live cells increased significantly with incubation time increasing, which indicated that both PLLA/0.5CNTs and PLLA scaffolds were favorable for cell proliferation. It should be noted that the PLLA/0.5CNTs scaffold exhibited a higher cell density than PLLA scaffold, indicating that it was more beneficial to cell growth.

The viability of cells incubated on PLLA/0.5CNTs and PLLA scaffolds was quantitatively assessed by CCK-8 assay, with results shown in Figure 10. It could be seen that the cell viability on PLLA/0.5CNTs and PLLA scaffolds increased with culture period extending from 1 to 7 days. In detail, the OD values increased from 0.6 to 2.8 for PLLA/0.5CNTs scaffold. Significantly, PLLA/0.5CNTs scaffolds presented enhanced OD values comparing with the PLLA scaffold at same time, which further proved that CNTs shown a positive effect on cell proliferation.

Basing on above cell experiments, it was indicated that PLLA/CNTs scaffold exhibited an enhanced cytocompatibility for cell adhesion and growth, as compared with PLLA scaffold. In general, cells were able to distinguish surfaces with different physical, chemistry and mechanical properties that directly affected cell behavior. As cells adhered to scaffold surface, they created a larger force at the adhesion site. It was believed that the PLLA/CNTs scaffold with stiffer matrix than PLLA scaffold could provide better cell adhesion. Secondly, the incorporation of CNTs into PLLA matrix resulted in the rough nano-scaled surface topography, which was more conducive for cell adhesion and growth [36]. In fact, rough surface was able to provide a variety of mechanical stimuli, thus promoting cell proliferation. Besides, the incorporated CNTs with excellent electrical properties could enhance the transmission of cell signals, thus promoting cell-cell communication and cellular activity [52].

4. Conclusions

In present study, CNTs were introduced into PLLA to improve the mechanical behavior. PLLA/CNTs scaffold was fabricated by SLS technique. CNTs enhanced the crystallinity of PLLA matrix due to its heterogeneous nucleation effect. More significantly, CNTs, as one-dimensional material, contributed to the crack bridging mechanism and pulling out effect. As a consequence, the obtained compressive strength, Vickers hardness and tensile strength of the scaffold were considerably enhanced from 5.6 to 6.8 MPa, 24.5 to 38.9 Hv, 15.5 to 18.6 MPa, respectively. Furthermore, PLLA/CNTs scaffold exhibited desirable biocompatibility. It was indicated that PLLA/CNTs scaffold was a promising candidate as bone implant.

Data Availability

The data used to support the findings of this study are available from the corresponding author upon request.

Conflicts of Interest

The authors declare that there are no conflicts of interest regarding the publication of this paper.

Authors' Contributions

Guoyong Wang and Fangwei Qi contributed equally in this work.

Acknowledgments

This study was supported by the following funds: (1) The Natural Science Foundation of China (51935014, 51905553, 81871494, 81871498, 51705540); (2) Hunan Provincial Natural Science Foundation of China (2019JJ50774, 2018JJ3671, 2019JJ50588); (3) JiangXi Provincial Natural Science Foundation of China (20192ACB20005); (4) Guangdong Province Higher Vocational Colleges & Schools Pearl River Scholar Funded Scheme (2018); (5) The Open Sharing Fund for the Large-scale Instruments and Equipments of Central South University; (6) The Project of Hunan Provincial Science and Technology Plan (2017RS3008); (7) The Natural Science Foundation of Jiangxi University Science and Technology (NSFJ2014-G29).

References

[1] P. Feng, J. He, S. Peng et al., "Characterizations and interfacial reinforcement mechanisms of multicomponent biopolymer based scaffold," *Materials Science and Engineering: C*, vol. 100, pp. 809–825, 2019.

[2] Z. Karimi, E. Seyedjafari, F. S. Mahdavi et al., "Baghdadite nanoparticle-coated Poly-L-Lactic Acid (PLLA) ceramics scaffold improved osteogenic differentiation of adipose tissue-derived mesenchymal stem cells," *Journal of Biomedical Materials Research Part A*, vol. 107, pp. 1284–1293, 2019.

[3] J. Feng, Z. Huang, and Y. Dong, "Effect of mixed solvents on the thermal properties of poly(L-lactic acid) (PLLA) solution and micromorphology of porous PLLA scaffolds," *Materials Research Express*, vol. 6, no. 1, p. 015314, 2018.

[4] D. Zhang, M. A. Kandadai, J. Cech, S. Roth, and S. A. Curran, "Poly (L-lactide)(PLLA)/multiwalled carbon nanotube (MWCNT) composite: characterization and biocompatibility evaluation," *The Journal of Physical Chemistry B*, vol. 110, no. 26, pp. 12910–12915, 2006.

[5] D. da Silva, M. Kaduri, M. Poley et al., "Biocompatibility, biodegradation and excretion of polylactic acid (PLA) in medical implants and theranostic systems," *Chemical Engineering Journal*, vol. 340, pp. 9–14, 2018.

[6] D. Vleggaar, R. Fitzgerald, Z. P. Lorenc et al., "Consensus recommendations on the use of injectable Poly-L-Lactic Acid for facial and nonfacial volumization," *Journal of Drugs in Dermatology*, vol. 13, no. 4, pp. s44–s51, 2014.

[7] D. J. Hickey, B. Ercan, L. Sun, and T. J. Webster, "Adding MgO nanoparticles to hydroxyapatite-PLLA nanocomposites for improved bone tissue engineering applications," *Acta Biomaterialia*, vol. 14, pp. 175–184, 2015.

[8] P. Feng, Y. Kong, L. Yu et al., "Molybdenum disulfide nanosheets embedded with nanodiamond particles: co-dispersion nanostructures as reinforcements for polymer scaffolds," *Applied Materials Today*, vol. 17, pp. 216–226, 2019.

[9] A. Pei, Q. Zhou, and L. A. Berglund, "Functionalized cellulose nanocrystals as biobased nucleation agents in poly(L-lactide) (PLLA): crystallization and mechanical property effects," *Composites Science and Technology*, vol. 70, no. 5, pp. 815–821, 2010.

[10] X. Hu, Y. Wang, L. Zhang, M. Xu, J. Zhang, and W. Dong, "Mechanical testing and reinforcing mechanisms of a magnetic field-sensitive hydrogel prepared by microwave-assisted polymerization," *Polymer Testing*, vol. 69, pp. 396–404, 2018.

[11] C. Shuai, J. Zan, F. Qi et al., "nMgO-incorporated PLLA bone scaffolds: Enhanced crystallinity and neutralized acidic products," *Materials & Design*, vol. 174, p. 107801, 2019.

[12] Y. Wang, X. Wang, Y. Xiang et al., "Hydroxyapatite-nanowires enhanced electrospun fiber via craze disperse stress for bone regeneration," *Nanoscience and Nanotechnology Letters*, vol. 10, no. 11, pp. 1498–1507, 2018.

[13] C. Gonçalves, A. Pinto, A. V. Machado, J. Moreira, I. C. Gonçalves, and F. Magalhães, "Biocompatible reinforcement of poly (lactic acid) with graphene nanoplatelets," *Polymer Composites*, vol. 39, pp. E308–E320, 2018.

[14] H.-B. Kim, D. K. Patel, Y.-R. Seo, and K.-T. Lim, "3D-printed scaffolds with reinforced poly (lactic acid)/carbon nanotube filaments based on melt extrusion," *Journal of Biosystems Engineering*, vol. 44, pp. 1–8, 2019.

[15] L. Valentini, S. B. Bon, M. Hernández, M. A. López-Manchado, and N. Pugno, "Nitrile butadiene rubber composites reinforced with reduced graphene oxide and carbon nanotubes show superior mechanical, electrical and icephobic properties," *Composites Science and Technology*, vol. 166, pp. 109–114, 2018.

[16] V. Amenta and K. Aschberger, "Carbon nanotubes: potential medical applications and safety concerns," *Wiley Interdisciplinary Reviews: Nanomedicine and Nanobiotechnology*, vol. 7, no. 3, pp. 371–386, 2015.

[17] Z.-M. Li, S.-N. Li, M.-B. Yang, and R. Huang, "A novel approach to preparing carbon nanotube reinforced thermoplastic polymer composites," *Carbon*, vol. 11, no. 43, pp. 2413–2416, 2005.

[18] X.-F. Wang, Z.-X. Zhang, J.-H. Yang, Y. Wang, and J.-H. Zhang, "{ZnO}@{ZnS} core/shell microrods with enhanced gas sensing properties," *RSC Advances*, vol. 5, no. 4, pp. 69522–69533, 2015.

[19] A. S. Mesgar, Z. Mohammadi, and S. Khosrovan, "Improvement of mechanical properties and in vitro bioactivity of freeze-dried gelatin/chitosan scaffolds by functionalized carbon nanotubes," *International Journal of Polymeric Materials and Polymeric Biomaterials*, vol. 67, no. 5, pp. 267–276, 2018.

[20] F. Luo, L. Pan, G. Hong et al., "In vitro and in vivo characterization of multi-walled carbon nanotubes/polycaprolactone composite scaffolds for bone tissue engineering applications," *Journal of Biomaterials and Tissue Engineering*, vol. 7, no. 9, pp. 787–797, 2017.

[21] Q. Cai, J. Mao, X. Li, and X. Yang, "Macroporous and nanofibrous {PLLA} scaffolds reinforced with calcium phosphate-coated multiwalled carbon nanotubes," *Materials Letters*, vol. 128, pp. 238–241, 2014.

[22] S. Ghorbani, H. Eyni, Z. Khosrowpour et al., "Spermatogenesis induction of spermatogonial stem cells using nanofibrous poly(L-lactic acid)/multi-walled carbon nanotube scaffolds and naringenin," *Polymers for Advanced Technologies*, 2019.

[23] Z. Fereshteh, *In Functional 3D Tissue Engineering Scaffolds*, pp. 151–174, Elsevier, Amsterdam, 2018.

[24] K. H. Tan, C. K. Chua, K. F. Leong et al., "Scaffold development using selective laser sintering of polyetheretherketone-hydroxyapatite biocomposite blends," *Biomaterials*, vol. 24, no. 18, pp. 3115–3123, 2003.

[25] C. Shuai, B. Wang, Y. Yang, S. Peng, and C. Gao, "3D honeycomb nanostructure-encapsulated magnesium alloys with superior corrosion resistance and mechanical properties," *Composites Part B: Engineering*, vol. 162, pp. 611–620, 2019.

[26] F. E. Wiria, C. K. Chua, K. F. Leong, Z. Y. Quah, M. Chandrasekaran, and M. W. Lee, "Improved biocomposite development of poly(vinyl alcohol) and hydroxyapatite for tissue engineering scaffold fabrication using selective laser sintering," *Journal of Materials Science: Materials in Medicine*, vol. 19, no. 3, pp. 989–996, 2008.

[27] H. Liang, Y. Yang, D. Xie et al., "Trabecular-like Ti-6Al-4V scaffolds for orthopedic: fabrication by selective laser melting and in vitro biocompatibility," *Journal of Materials Science & Technology*, vol. 35, no. 7, pp. 1284–1297, 2019.

[28] Y. Cao, T. Shi, C. Jiao et al., "Fabrication and properties of zirconia/hydroxyapatite composite scaffold based on digital light processing," *Ceramics International*, 2019.

[29] Y. Yang, F. Yuan, C. Gao et al., "A combined strategy to enhance the properties of Zn by laser rapid solidification and laser alloying," *Journal of the Mechanical Behavior of Biomedical Materials*, vol. 82, pp. 51–60, 2018.

[30] Y. Zhou, L. Lei, B. Yang, J. Li, and J. Ren, "Preparation and characterization of polylactic acid (PLA) carbon nanotube nanocomposites," *Polymer Testing*, vol. 68, pp. 34–38, 2018.

[31] C.-C. Chen, J.-Y. Chueh, H. Tseng, H.-M. Huang, and S.-Y. Lee, "Preparation and characterization of biodegradable PLA polymeric blends," *Biomaterials*, vol. 24, no. 7, pp. 1167–1173, 2003.

[32] S. Liu, G. Wu, and Y. Xiao, "Multi-interfaces investigation on the PLA composites toughened by modified MWCNTs," *Composite Interfaces*, vol. 24, no. 8, pp. 743–759, 2017.

[33] S. L. Rebelo, A. Guedes, M. E. Szefczyk, A. M. Pereira, J. P. Araújo, and C. Freire, "Progress in the Raman spectra analysis of covalently functionalized multiwalled carbon nanotubes: unraveling disorder in graphitic materials," *Physical Chemistry Chemical Physics*, vol. 18, no. 18, pp. 12784–12796, 2016.

[34] Z. Xu, Y. Niu, L. Yang et al., "Morphology, rheology and crystallization behavior of polylactide composites prepared through addition of five-armed star polylactide grafted multiwalled carbon nanotubes," *Polymer*, vol. 51, no. 3, pp. 730–737, 2010.

[35] C. Shuai, Y. Xu, P. Feng, G. Wang, S. Xiong, and S. Peng, "Antibacterial polymer scaffold based on mesoporous bioactive glass loaded with in situ grown silver," *Chemical Engineering Journal*, vol. 374, pp. 304–315, 2019.

[36] L. Pan, X. Pei, R. He, Q. Wan, and J. Wang, "Multiwall carbon nanotubes/polycaprolactone composites for bone tissue engineering application," *Colloids and Surfaces B: Biointerfaces*, vol. 93, pp. 226–234, 2012.

[37] T. Huang, J.-H. Yang, N. Zhang, J.-H. Zhang, and Y. Wang, "Highly efficient non-fullerene polymer solar cells enabled by novel non-conjugated small-molecule cathode interlayers," *Polymer Bulletin*, vol. 75, pp. 2641–2655, 2018.

[38] C. Shuai, Y. Cheng, Y. Yang, S. Peng, W. Yang, and F. Qi, "Laser additive manufacturing of Zn-2Al part for bone repair: formability, microstructure and properties," *Journal of Alloys and Compounds*, vol. 798, pp. 606–615, 2019.

[39] C. Gao, M. Yao, C. Shuai, S. Peng, and Y. Deng, "Nano-SiC reinforced Zn biocomposites prepared via laser melting: microstructure, mechanical properties and biodegradability," *Journal of Materials Science & Technology*, vol. 35, no. 11, pp. 2608–2617, 2019.

[40] S. Wong, R. A. Shanks, and A. Hodzic, "Mechanical behavior and fracture toughness of poly (L-lactic acid)-natural fiber composites modified with hyperbranched polymers," *Macromolecular Materials and Engineering*, vol. 289, no. 5, pp. 447–456, 2004.

[41] M. Xing, *Cardiac Regeneration and Repair*, pp. 3–16, Elsevier, Amsterdam, 2014.

[42] H. H. Bayraktar, E. F. Morgan, G. L. Niebur, G. E. Morris, E. K. Wong, and T. M. Keaveny, "Comparison of the elastic and yield properties of human femoral trabecular and cortical bone tissue," *Journal of Biomechanics*, vol. 37, no. 1, pp. 27–35, 2004.

[43] I. Srivastava and N. Koratkar, "Fatigue and fracture toughness of epoxy nanocomposites," *Journal of Management*, vol. 62, no. 2, pp. 50–57, 2010.

[44] S. H. Park and P. R. Bandaru, "Improved mechanical properties of carbon nanotube/polymer composites through the use of carboxyl-epoxide functional group linkages," *Polymer*, vol. 51, no. 22, pp. 5071–5077, 2010.

[45] V. Mirjalili and P. Hubert, "Modelling of the carbon nanotube bridging effect on the toughening of polymers and experimental verification," *Composites Science and Technology*, vol. 70, no. 10, pp. 1537–1543, 2010.

[46] Y. Liu and S. Kumar, "Polymer/carbon nanotube nano composite fibers–a review," *ACS Applied Materials & Interfaces*, vol. 6, no. 9, pp. 6069–6087, 2014.

[47] Z. Qi, Y. Tan, Z. Zhang, L. Gao, C. Zhang, and J. Tian, "Synergistic effect of functionalized graphene oxide and carbon nanotube hybrids on mechanical properties of epoxy composites," *RSC Advances*, vol. 8, no. 67, pp. 38689–38700, 2018.

[48] L. Aliotta, P. Cinelli, M. B. Coltelli, M. C. Righetti, M. Gazzano, and A. Lazzeri, "Effect of nucleating agents on crystallinity and properties of poly (lactic acid) (PLA)," *European Polymer Journal*, vol. 93, pp. 822–832, 2017.

[49] C. Gao, M. Yao, S. Li, P. Feng, S. Peng, and C. Shuai, "Highly biodegradable and bioactive Fe-Pd-bredigite biocomposites prepared by selective laser melting," *Journal of Advanced Research*, vol. 20, pp. 91–104, 2019.

[50] C. Shuai, S. Li, S. Peng, P. Feng, Y. Lai, and C. Gao, "Biodegradable metallic bone implants," *Materials Chemistry Frontiers*, vol. 3, pp. 544–562, 2019.

[51] Y. Yang, C. He, E. Dianyu et al., "Mg bone implant: features, developments and perspectives," *Materials & Design*, p. 108259, 2019.

[52] W. Wang, B. Huang, J. J. Byun, and P. Bartolo, "Assessment of PCL/carbon material scaffolds for bone regeneration," *Journal of the Mechanical Behavior of Biomedical Materials*, vol. 93, pp. 52–60, 2019.